

Adapting coherent-state superpositions in noisy channels

Jan Provazník^{1*}, Petr Marek¹, Julien Laurat², Radim Filip¹

¹ *Department of Optics, Palacký University, 17. listopadu 1192/12, 771 46 Olomouc, Czech Republic*

² *Laboratoire Kastler Brossel, Sorbonne Université, CNRS, ENS-Université PSL, Collège de France, 4 place Jussieu, 75005 Paris, France*

* provaznik@optics.upol.cz

Abstract: Quantum non-Gaussian states are crucial for the fundamental understanding of non-linear bosonic systems and simultaneously advanced applications in quantum technologies. In many bosonic experiments the important quantum non-Gaussian feature is the negativity of the Wigner function, a cornerstone for quantum computation with bosons. Unfortunately, the negativities present in complex quantum states are extremely vulnerable to the effects of decoherence, such as energy loss, noise and dephasing, caused by the coupling to the environment, which is an unavoidable part of any experimental implementation. An efficient way to mitigate its effects is by adapting quantum states into more resilient forms. We propose an optimal protection of superpositions of coherent states against a sequence of asymmetric thermal lossy channels by suitable squeezing operations.

1 Introduction

Fault tolerant quantum computation is one of the main goals of quantum information science [1–3]. Traveling light fields offer unprecedented scalability [4–8] and have been already used to demonstrate a path towards quantum advantage [2]. There, the information is encoded into non-Gaussian superpositions of quantum states [9–12]. Coherent Schrödinger (CS) states, defined as quantum superposition of coherent states with different amplitudes can be considered an elementary version of such codes [4, 13–16], and they can be also employed in quantum communication protocols [17–20], quantum sensing [21] and spectroscopy [22].

The main challenge faced by the optical systems is the decoherence, mainly optical loss and thermal noise. While high quality quantum states may offer the possibility of error correction [9–12], decoherence poses severe limits on the preparation and propagation of such states [23, 24]. While energy loss can never completely remove certain quantum non-Gaussian features from quantum states [25], losing half of the signal to the environment is enough to completely obliterate any negativity of the Wigner function, thus preventing any possibility of quantum advantage [26]. Loss combined with noise present in the environment makes its decay even faster.

It has been established that the effects of loss in photon qubit systems can be probabilistically mitigated by suitable pre-processing of optical signals [27–29] or channel engineering [30]. Most auspiciously, CS states specifically can be made more resilient to loss by applying a suitable deterministic squeezing operation [31–37]. Specifically, it has been shown for pure lossy channels in [35]. However, to what extent can these methods be used for mitigation of added channel noise together with loss has not been studied so far.

To address this question we consider a CS state propagating through a general series of channels incorporating loss and added phase-sensitive noise. We derive a general condition that needs to be satisfied to preserve any negativity present in the Wigner function of the quantum state based on optimal deterministic squeezing operations, that maximizes the central negativity of the Wigner

function. In addition we extend the general condition to include even-parity CS states in the form of a necessary condition that must be satisfied for any negative values of the Wigner function to exist.

Our analysis based on negativity of the Wigner function is complemented by adapting the squeezing operations to maximize the Hilbert-Schmidt distance between CS states of opposite parities transmitted through the decohering channels.

2 Minimizing decoherence in a single noisy channel

Potential applications of CS states in quantum computation protocols range from their direct use [13–17, 38], through error correction [39] to GKP state production, where they serve the important role of non-Gaussian building blocks [9, 40, 41]. Their versatility comes from their non-Gaussian features that diminish in the presence of Gaussian loss [31–37] and additive noise.

Our search for methods capable of increasing their resilience against noise starts by considering a single lossy single channel with added noise, schematically depicted in Figure 1. The channel can be modeled with an unbalanced beam splitter where the transmitted signal interacts with the environment in a generally asymmetrical thermal state, which can be understood as an initially symmetric thermal state that underwent squeezing. In our model we assume that the parameters of the channel are known.

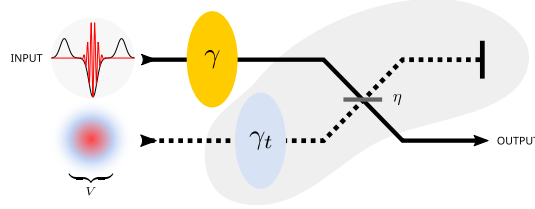


Figure 1. The signal (solid line) is transmitted through a lossy channel represented by a beam splitter with transmittance η where it interacts with the environment (dashed line). The environment is assumed to be in an axis-aligned asymmetric thermal state, which can be interpreted as a symmetric thermal state characterized by its variance V and the associated squeezing rate γ_t . The signal state can be protected against decoherence with an optional pre-squeezing operation. Its squeezing rate γ can be adapted to offer the best protection of the transmitted CS state.

The CS states propagating through the channel are defined as quantum superpositions of two coherent states with identical amplitudes and opposite phases. We recognize two types of CS states based on their parity,

$$|\xi, \pm\rangle = \frac{1}{\sqrt{2}} \frac{|\xi\rangle \pm |-\xi\rangle}{\sqrt{1 \pm \exp(-2|\xi|^2)}} \quad (1)$$

where $|\xi\rangle$ denotes coherent states — eigenstates of the annihilation operator \hat{a} . The symbol $|\xi, +\rangle$ stands for the even-parity and $|\xi, -\rangle$ the odd-parity CS state. Their respective Wigner functions, defined in variables corresponding to quadrature operators with $[\hat{x}, \hat{p}] = i$, read

$$W_{\xi, \pm}(X, P) = \frac{1}{2} \frac{w_{\xi, \xi}(X, P) \pm [w_{\xi, -\xi}(X, P) + w_{-\xi, \xi}(X, P)] + w_{-\xi, -\xi}(X, P)}{1 \pm \exp(-2|\xi|^2)}. \quad (2)$$

They are expressed in terms of the complex-exponential building blocks

$$\begin{aligned} w_{\xi,\xi}(X,P) &= \frac{1}{\pi} \exp\left(-(X-X_0)^2 - (P-P_0)^2\right), \\ w_{\xi,-\xi}(X,P) &= \frac{1}{\pi} \exp\left(-(X-\imath P_0)^2 - (P+\imath X_0)^2\right) \exp\left(-2|\xi|^2\right), \end{aligned} \quad (3)$$

where we set $\sqrt{2}\xi \equiv X_0 + \imath P_0$ and therefore $2|\xi|^2 \equiv X_0^2 + P_0^2$. As for the final building block, omitted in (3), we have $w_{-\xi,\xi}(X,P) \equiv \text{conj}\{w_{\xi,-\xi}(X,P)\}$. These two complex-exponential blocks add up to a real-valued cosine.

The Wigner function $W'_{\xi,\pm}(X',P')$ of the transmitted state is given by the integral transform

$$W'_{\xi,\pm}(X',P') = \iint W_{\xi,\pm}(X,P) K(X,P,X',P') dX dP \quad (4)$$

of its initial Wigner function $W_{\xi,\pm}(X,P)$ with the kernel function $K(X,P,X',P')$ representing the quantum channel. The Gaussian channels under our consideration can be described with

$$K(X,P,X',P') = \frac{\pi^{-1}}{\sqrt{\sigma_X \sigma_P}} \exp\left(-\frac{(X' - f_X X)^2}{\sigma_X} - \frac{(P' - f_P P)^2}{\sigma_P}\right) \quad (5)$$

where $f_X, f_P, \sigma_X, \sigma_P \in \mathbb{R}$ parametrize the channel. Their exact values depend on the particular channel. The kernel function (5) accommodates a broader range of channels beyond loss, including those where the transmitted states are squeezed before and after their interaction with the environment. It is, however, limited to channels preserving the separability of the quadrature variables. In our analysis we only consider channels with thermal environment, where the thermal state is axis-aligned with the transmitted CS state. This can be guaranteed by using a phase-shift operation before their transmission.

When a CS state propagates through the channel (5), the blocks (3) transform into

$$\begin{aligned} w'_{\xi,\xi}(X',P') &= \frac{1}{\pi} \frac{1}{\sqrt{V_X V_P}} \exp\left(-\frac{(X' - f_X X_0)^2}{V_X} - \frac{(P' - f_P P_0)^2}{V_P}\right), \\ w'_{\xi,-\xi}(X',P') &= \frac{1}{\pi} \frac{1}{\sqrt{V_X V_P}} \exp\left(-\frac{(X' - \imath f_X P_0)^2}{V_X} - \frac{(P' + \imath f_P X_0)^2}{V_P}\right) \exp\left(-2|\xi|^2\right), \end{aligned} \quad (6)$$

where $V_X = \sigma_X + f_X^2$ and $V_P = \sigma_P + f_P^2$. Together these form the transformed Wigner function

$$W'_{\xi,\pm}(X',P') = \frac{1}{2} \frac{w'_{\xi,\xi}(X',P') \pm [w'_{\xi,-\xi}(X',P') + w'_{-\xi,\xi}(X',P')] + w'_{-\xi,-\xi}(X',P')}{1 \pm \exp(-2|\xi|^2)} \quad (7)$$

with structure similar to the initial Wigner function (2) since both the integral kernel (4) and the complex-exponential fragments (3) are Gaussian functions separable in terms of X and P .

It has been established [34–36] that the rapid decay of negative values in Wigner functions of CS states due to pure loss (vacuum environment) can be mitigated with adaptive pre-squeezing operation prior to their transmission through the lossy channel.

Channels of this kind, depicted in Figure 1, can be characterized with parameters

$$\begin{aligned} f_X &= \sqrt{\eta} e^{-\gamma}, & \sigma_X &= 2(1-\eta) e^{-2\gamma} V, \\ f_P &= \sqrt{\eta} e^{+\gamma}, & \sigma_P &= 2(1-\eta) e^{+2\gamma} V. \end{aligned} \quad (8)$$

where γ gives the squeezing rate of the pre-squeezing operation applied to the signal state, η defines the (intensity) transmittance of the channel. The signal is mixed with the environment,

an asymmetric thermal state, which can be parametrized by its initial symmetric variance V and squeezing rate γ_t of the asymmetrizing operation. Asymmetric thermal states remain classical for squeezing rates $|\gamma_t| \leq \log \sqrt{V}$ as neither quadrature variance, $V_{\pm} = \exp(\pm 2\gamma_t)V$, becomes squeezed below the vacuum threshold. The environment noise becomes non-classical beyond this limit.

Negative Wigner functions exclude Gaussian behavior of quantum states [42, 43]. One of the prominent features of odd-parity CS states is the central negativity of their Wigner function. While central negativity is only a sufficient condition for quantum non-Gaussianity [43], its reduction can be used as a qualitative indicator of observability of the transmitted CS state above measurement and statistical noise [35, 37]. It also offers an experimental advantage as its measurement does not require a full state tomography [44–47]. In optics, its value can be obtained directly as an expectation value of the photon number parity operator [48] or computed from its photon number distribution [49].

Central negativity (CN) of the Wigner function of the odd-parity CS state is readily obtained from the transformed Wigner function (7) as

$$W'_{\xi,-}(0,0) = f_{\xi,-} \left\{ \exp \left(-\frac{f_X^2}{V_X} X_0^2 - \frac{f_P^2}{V_P} P_0^2 \right) - \exp \left(-\frac{\sigma_X}{V_X} P_0^2 - \frac{\sigma_P}{V_P} X_0^2 \right) \right\} \quad (9)$$

where the normalization factor reads $f_{\xi,-}^{-1} = \pi \sqrt{V_X V_P} (1 - \exp(-2|\xi|^2))$. It will be negative iff

$$f_X^2 f_P^2 - \sigma_X \sigma_P > 0. \quad (10)$$

This criterion can be generalized to include even-parity states at the cost of sufficiency. If the transformed Wigner function (7) of the transmitted CS state is to attain negative values anywhere, the channel must necessarily satisfy $f_X^2 f_P^2 - \sigma_X \sigma_P > 0$. In particular,

$$\exists (X, P) \in \mathbb{R}^2 : W'_{\xi,\pm}(X, P) < 0 \implies f_X^2 f_P^2 - \sigma_X \sigma_P > 0. \quad (11)$$

This condition is both necessary and sufficient for the central negativity of odd-parity CS states. Alternatively the necessary condition, equivalent to (11),

$$f_X^2 f_P^2 - \sigma_X \sigma_P < 0 \implies \forall (X, P) \in \mathbb{R}^2 : W_{\xi,\pm}(X, P) > 0 \quad (12)$$

precludes negativity anywhere within the Wigner function (7). Both conditions are independent of the magnitude and parity of the transmitted CS state and depend only on the parameters of the channel. Both statements are proven and discussed within the supplementary material.

In the context of channels (8), depicted in Figure 1, the condition (11) provides a connection between the beam splitter transmittance η and the symmetric variance V of the thermal state. It establishes a region of feasible parameters of the lossy channel, independent of γ_t , bounded by

$$\frac{2V}{1+2V} < \eta < 1 \quad \text{and} \quad 0 < V < \frac{\eta}{2(1-\eta)}, \quad (13)$$

where the negativities in the transmitted state survive. No amount of pre-squeezing γ is going to protect CS states transmitted through channels (8) with parameters outside of this region.

In Figure 2 we consider lossy channels (8) with varying transmission rates and different asymmetries $\gamma_t \in \{-3, -1, 1, 3\}$ dB of the channel noise characterized by $V = 1$, corresponding to a thermal state with double the variance of a vacuum state. An odd-parity CS state with $\sqrt{2}\xi = 3$ is transmitted through the channel. The amplitude ξ of the input CS state was chosen to be real number without a loss of generality as the state can be arbitrarily rotated in the phase space before its transmission. The colored dashed lines in Figure 2 (a) represent CN of the state transmitted without any protection. The optimal squeezing rates of the protective pre-squeezing are determined by performing a numerical optimization of (9) with respect to γ . The solid black line represents the best attainable CN when

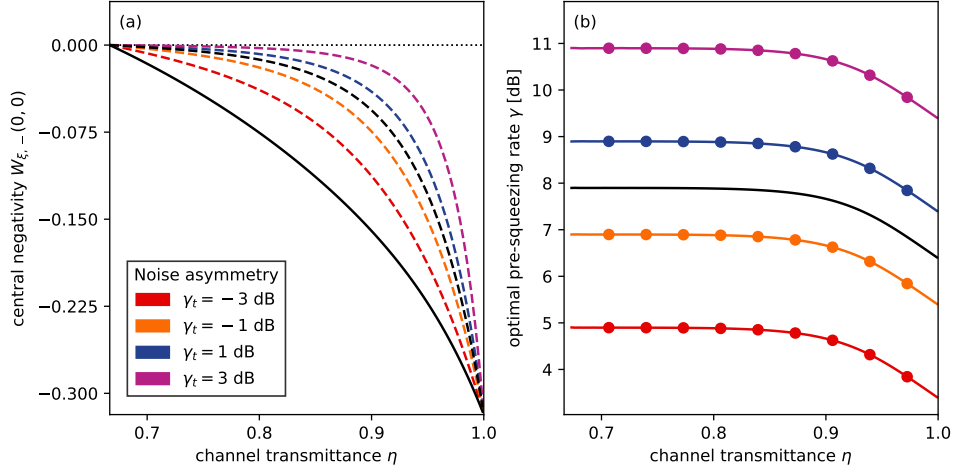


Figure 2. Adaptive pre-squeezing protects odd-parity CS state (with $\sqrt{2}\xi = 3$) from decoherence due to loss and thermal noise with varying asymmetry. **(a)** Dashed lines represent CN without protection. Asymmetries of the thermal noise with $V = 1$ (twice the variance of the vacuum state) are represented with different colors. We use black for the symmetric case with $\gamma_t = 0$, red for $\gamma_t = 1$ dB, orange for $\gamma_t = 3$ dB, blue for $\gamma_t = 5$ dB, and purple for $\gamma_t = 6$ dB asymmetric cases. The solid black line represents the best attainable CN and does not depend on the γ_t rate of the asymmetry. **(b)** Optimal pre-squeezing rates γ follow the same color scheme. Colored lines represent optimal rates for different asymmetries. The lines appear constantly shifted by the value of γ_t from the solid black line, which represents the optimal pre-squeezing γ found for the symmetric thermal state ($\gamma_t = 0$). The colored bullet points correspond to γ_t added to its values at regular intervals to emphasise the constant shifts.

the state is optimally pre-squeezed prior to its transmission. It does not depend on the asymmetry γ_t of the thermal state and coincides with the best attainable CN obtained for the symmetric thermal state. The corresponding optimal squeezing rates γ are shown in Figure 2 (b). The solid black line represents the optimal pre-squeezing for the symmetric thermal state, whereas the colored solid lines represent different asymmetries of the state. The lines in the figure are shifted by constant offsets equal to the squeezing rate γ_t of the asymmetry. This observation is supported by the colored bullet points which were obtained by adding the respective values of γ_t to the optimal values of γ obtained for the symmetric thermal state.

The optimal protective pre-squeezing operation can be interpreted as a pair of virtual squeezing operations with rates γ_0 and γ_1 , joined together into a single physical squeezing operation with $\gamma = \gamma_0 + \gamma_1$ rate. The first virtual squeezer, with γ_0 , realizes the protective pre-squeezing of the transmitted CS state, while the other squeezer, with squeezing rate $\gamma_1 \equiv \gamma_t$, reshapes the pre-squeezed state to match the asymmetry of the environment. Inverse squeezing operation can be applied after the channel to reshape the Wigner function back into its initial form without altering the non-Gaussian properties of the transmitted CS state. The optimal squeezing rate γ_0 of the protective pre-squeezing operation itself depends on the CS state, the excess of the thermal noise and the transmittance of the channel. It must be determined numerically on a case by case basis.

We can also interpret the reshaping of the state, performed by the second virtual squeezer, as a

symmetrization of the environment. The second virtual squeezing operation γ_1 performed on the state and the virtual squeezing γ_t of the thermal state share an identical squeezing rate. Consequently, the two squeezing operations can be propagated through the beam splitter in Figure 1, thus reducing the resulting effective scheme to the actual protective pre-squeezing operation and a regular loss channel with a symmetric thermal noise. This interpretation allows us to focus solely on cases with symmetric noise.

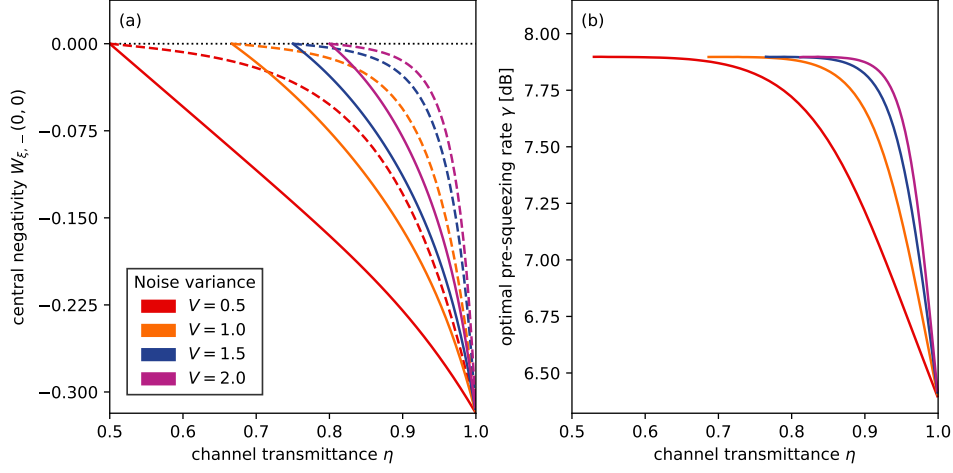


Figure 3. Adaptive pre-squeezing protects odd-parity CS state (with $\sqrt{2}\xi = 3$) from decoherence due to loss and thermal noise. We consider symmetric thermal noise, characterized by its variance $V \in \{0.5, 1.0, 1.5, 2.0\}$. Colors are used to distinguish between individual variances. **(a)** Dashed lines represent CN without protection. Solid lines correspond to CN attained by optimally pre-squeezed CS states. **(b)** Optimal pre-squeezing rate γ does not exhibit trivial dependence on the variance V of the thermal noise.

In Figure 3 we investigate the adaptation of an odd-parity CS state with $\sqrt{2}\xi = 3$ transmitted through the lossy channel (8) with different amounts of symmetric thermal noise, characterized by its variance $V \in \{0.5, 1.0, 1.5, 2.0\}$, where the thermal state with $V = 0.5$ corresponds to pure loss. In Figure 3 (a) we show the best attainable CN of odd-parity states. We employ the condition (13) to determine the least viable transmittance and only present the results where the transmitted CS state exhibits CN. The dashed lines represent cases without any protective pre-squeezing, whereas the solid lines, corresponding to the optimal adaptation of the transmitted CS state, exhibit significantly improved CN. In Figure 3 (b) we present the optimal squeezing rates γ of the pre-squeezing operation. The optimal squeezing rate γ does not exhibit trivial dependence on the variance V and must be determined numerically on a case by case basis.

Adverse effects of asymmetric thermal noise can be mitigated with squeezing operations adapted to the asymmetry and the overall amount of the thermal noise in addition to adaptation for the loss rate and the transmitted CS state itself. The adaptation process can be understood as a combination of the protective pre-squeezing in the sense of [34–36] and an additional squeezing operation, which effectively removes the asymmetry. Consequently, in the analytical models used for the optimization, we can freely replace the lossy channels with asymmetrical thermal environment by lossy channels with equivalent symmetrical thermal noise.

Quantum states can propagate through diverse environments during their lifetime. To further our analysis we consider a natural extension to sequences of lossy quantum channels.

3 Minimizing decoherence across multiple noisy channels

Composite quantum channels could prove to be advantageous by permitting complex mitigation strategies with protective operations potentially accessing the intermediate channel (channels) in the middle. Conversely, should no such complex mitigation protocol exist, adaptation of the state to the composite channel performed only at its beginning would still remain optimal.

A sequence of Gaussian channels (5) can be concatenated together to form another Gaussian channel which can be described with the same formalism. Similarly a Gaussian channel (5) can be decomposed into more Gaussian channels [50]. Simple decohering Gaussian channels have been extensively discussed in the literature [34–36], as well as in the previous section with some useful observations about symmetrization of the environment.

Protection of CS states against decoherence may benefit from intermediate squeezing in composite channels. Consider the channel illustrated in Figure 4. The signal CS state is pre-squeezed, passes through the first beam splitter. It is squeezed again before passing through the second beam splitter. It may be optionally squeezed as it leaves the channel, however, the final squeezing does not affect the central negativity of odd-parity CS states we use in our analysis. Its parametrization in terms of the formalism of (5) is given by

$$\begin{aligned} f_X &= \sqrt{\eta\eta'} e^{-(\gamma+\gamma')} , \\ \sigma_X &= 2(1-\eta')e^{-2\gamma'_t}V' + 2\eta'(1-\eta)e^{-2(\gamma'+\gamma_t)}V , \\ f_P &= \sqrt{\eta\eta'} e^{+(\gamma+\gamma')} , \\ \sigma_P &= 2(1-\eta')e^{+2\gamma'_t}V' + 2\eta'(1-\eta)e^{+2(\gamma'+\gamma_t)}V' , \end{aligned} \quad (14)$$

where the transmittances of the channels are given by η and η' , the pre-squeezing rate is γ and the intermediate mid-squeezing rate is γ' . The first thermal noise is described by the symmetric variance V and the asymmetrizing squeezing γ_t . Similarly the second thermal noise is characterized by V' and γ'_t .

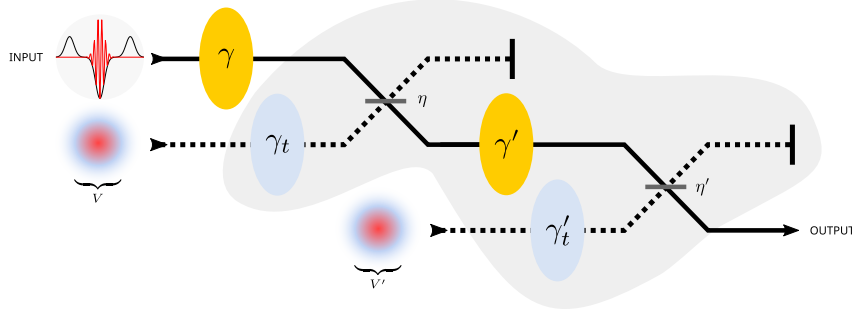


Figure 4. Illustration of a composite channel comprising a pair of lossy channels with pre-squeezing (γ) and mid-squeezing (γ'). The first channel is parametrized by (V, γ_t) describing the asymmetric thermal state and η determining its transmittance. Parameters of the second channel are distinguished by primes.

In Figure 5 we explore the central negativity of the odd-parity CS state with $\sqrt{2}\xi = 3$ transmitted through a composite channel (14). Without loss of generality we set the transmittances in both channels identical to keep the visualisation two dimensional. The plots show the best attainable negativity and the optimal pre-squeezing and mid-squeezing rates. We consider a number of asymmetric thermal environments. In Figure 5 (a) the dashed lines represent the attainable CN without

any protective squeezing operations applied. The solid black line represents the best attainable CN when optimal pre-squeezing and mid-squeezing operations are applied to the CS state. The optimal CN depends only on the symmetric variance of the noise, rather than its asymmetry. The solid black line can be equally obtained for the same channel where both environments are symmetric. The solid black line in Figure 5 (b) represents the optimal pre-squeezing rate γ obtained when there is no asymmetry in either thermal environment, whereas the colored lines correspond to different asymmetries. We recognize that these rates are constantly shifted from the symmetric case, the offset equal to γ_t of the first channel. The colored bullets, obtained by adding the respective γ_t rates to the black line, are used to highlight this observation. Furthermore, in the third plot, Figure 5 (c), we observe that the optimal mid-squeezing rates γ' match the differences $\gamma' \equiv \gamma'_t - \gamma_t$ between the asymmetries of both environments.

We can interpret the pre-squeezing operation as a pair of virtual squeezing operations, as we did previously in the discussion of single channels, where the first virtual squeezer, with squeezing rate γ_0 realizes the actual protective pre-squeezing, whereas the second one reshapes the transmitted state to match the asymmetry of the environment in the first channel. The mid-squeezing operation can be also understood as a composition of two squeezers, where the first squeezer transforms the transmitted state back to its original shape, while the second one reshapes it once again to match the asymmetry of the environment within the second channel. Interestingly, we can also obtain the optimal mid-squeezing rate γ' by maximizing the necessary condition (11).

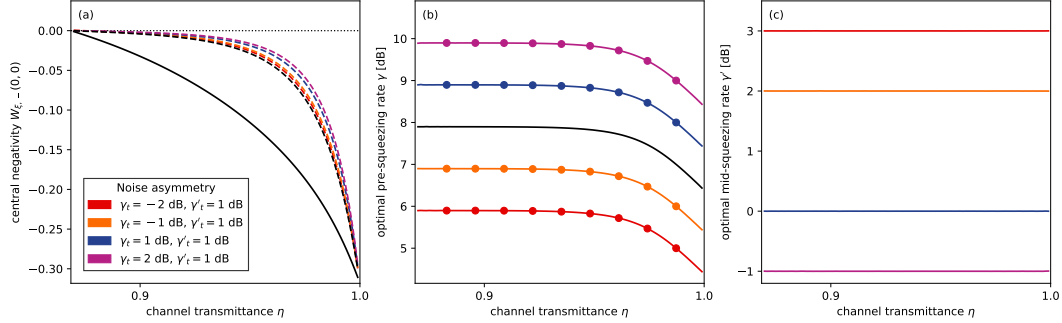


Figure 5. Adaptive squeezing protects odd-parity CS state ($\sqrt{2}\xi = 3$) from decoherence due to interaction with asymmetric thermal states with $V = 1$, $\gamma_t = \{-2, -1, 1, 2\}$ dB in the first channel and $V' = 2$, $\gamma'_t = 1$ dB in the second channel. Solid black lines represent the cases where both thermal states are symmetric. **(a)** Attainable central negativity. Dashed lines represent the attainable negativity without any adaptation. After adaptation, a part of which effectively symmetrizes the environment, the best attainable negativities coincide. The solid black line determines this best attainable negativity. **(b)** Optimal pre-squeezing rate γ_t where the solid black line represents the optimal adaptation in the fundamental case when both thermal states of the environment are symmetric. Colored lines correspond to optimal pre-squeezing rates for asymmetric environments. These lines are shifted by a constant offset equal to γ_t . This fact is emphasized by the colored bullets that are obtained by adding γ_t to the fundamental pre-squeezing rate represented by the solid black line. **(c)** Optimal mid-squeezing rate γ'_t depends only on the asymmetry of the adjacent thermal states. Its value is determined by the difference $\gamma'_t - \gamma_t$.

Because the optimal mid-squeezing rate depends solely on the asymmetries of individual en-

vironments, the composite channel (14) can be reduced into a single elementary channel (8) with effective transmittance η_e and thermal noise variance V_e given by

$$\begin{aligned}\eta_e &= \eta\eta' , \\ V_e &= \frac{(1 - \eta')V' + (1 - \eta)\eta'V}{1 - \eta\eta'} .\end{aligned}\tag{15}$$

This brings the entire analysis of composite channels back to the previous discussion of elementary channels. The protection of the CS state is facilitated **entirely** by the initial pre-squeezing operation and composite channels (14) can be substituted with equivalent elementary channels (8) parametrized by (15). Consequently, it is sufficient to only analyse noisy lossy channels with symmetric thermal environment.

With these conclusions in mind, we turn our attention back to the case of a single lossy channel with symmetric thermal noise and consider an alternative way of measuring the quality of the protection offered by the pre-squeezing operation.

4 Hilbert-Schmidt distance as a measure of state adaptation

The appeal of the central negativity of the odd-parity CS state stems from its availability as it can be measured directly or straightforwardly estimated. The presence of negativity within the Wigner function is also a necessary condition for the presence of quantum non-Gaussianity in the transmitted state [42, 43], contextuality [51] and advanced quantum protocols [52]. It also establishes a bound on the rest of the negative regions of Wigner function of the odd-parity CS state. However, because it is a local measure, it does not provide sufficient information about the other negative regions of the Wigner function of the transmitted CS state and its other quantum non-Gaussian aspects.

To complete the analysis, we use a directly measurable [53–56] Hilbert-Schmidt distance [57] between opposite-parity CS states transmitted through the channel (8). These two states form an orthonormal computational basis in quantum computation protocols [13–17, 38]. Their orthogonality can be measured with the Hilbert-Schmidt distance; it deteriorates as their quantum non-Gaussian features decay due to decoherence. While the distance itself does not directly indicate presence of quantum non-Gaussian features, our analysis determines whether the distance between the states can be improved through CS state adaptation.

The Hilbert-Schmidt distance

$$\begin{aligned}\Delta_\xi &= 2\pi \iint_{\mathbb{R}^2} \left[W'_{\xi,+}(X, P) - W'_{\xi,-}(X, P) \right]^2 dXdP \\ &= P_{\xi,+} - 2Q_\xi + P_{\xi,-}\end{aligned}\tag{16}$$

is defined in terms of Wigner functions (7) and effectively pits the purities $P_{\xi,\pm}$ of the transmitted CS states against their mutual overlap Q_ξ . The distance is bounded, $0 \leq \Delta_\xi \leq 2$, both from below and above. It can be expressed analytically. The final analytical expression is provided in the supplementary material.

In Figure 6 we investigate the Hilbert-Schmidt distance for a particular CS state with $\sqrt{2}\xi = 3$ magnitude transmitted through an elementary channel (8). It was established in prior sections that it is optimal to adapt the state to the asymmetry of the environment, or to equally symmetrize the environment. Consequently we consider only symmetric environment with distinct amount of thermal noise characterized by its variance $V \in \{0.5, 1.0, 1.5, 2.0\}$ where $V = 0.5$ corresponds to pure loss. The attainable Hilbert-Schmidt distance is presented in Figure 6 (a) where different colors encode different variances of the thermal noise. Dashed lines represent the distance obtained without the protective pre-squeezing operation, whereas the solid lines correspond to optimally pre-squeezed

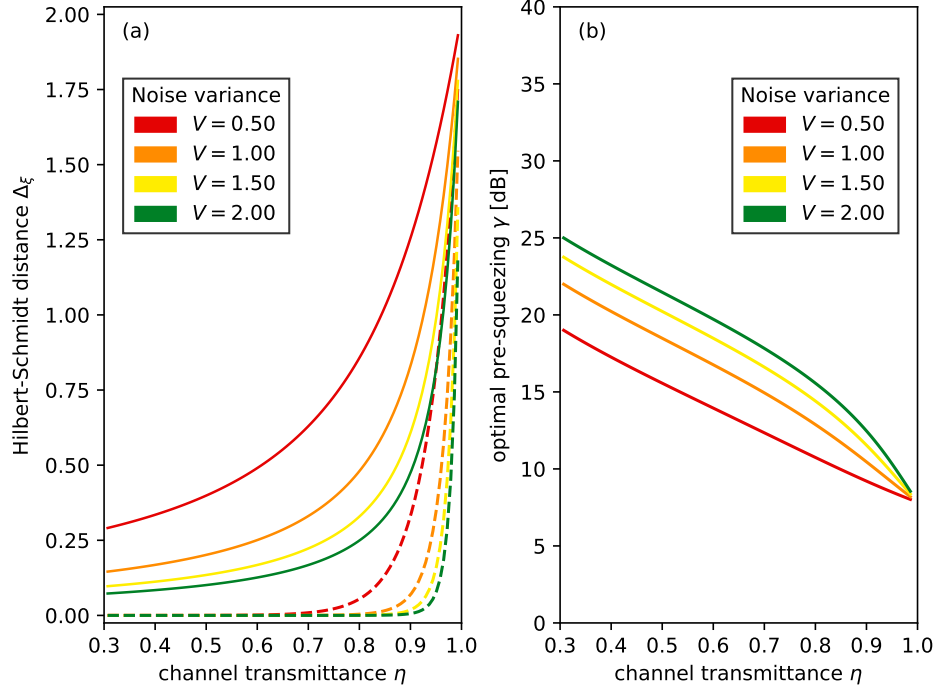


Figure 6. Hilbert-Schmidt distance Δ_ξ between opposite-parity CS states (with $\sqrt{2}\xi = 3$) transmitted through the channel (8) where the environment is a symmetric thermal noise with variance $V \in \{0.5, 1.0, 1.5, 2.0\}$. Colors indicate different thermal variance. **(a)** The attainable Hilbert-Schmidt distance without protective pre-squeezing is represented with dashed lines, whereas the solid lines correspond to optimally pre-squeezed CS states. We can surmise that pre-squeezing certainly offers advantage as the attainable distance between the transmitted states is greater. **(b)** The optimal pre-squeezing rate used to protect the CS states before their transmission.

CS states. The adaptation is certainly advantageous as the distance between the transmitted CS states is lower without the protective pre-squeezing. The optimal pre-squeezing rates, presented in Figure 6 (b), do not depend trivially on the amount of the noise and must be determined numerically on a case by case basis.

The Hilbert-Schmidt distance between transmitted CS states with opposite parities can be used to measure the protective effects of the adaptive pre-squeezing operation. This measure successfully complements analysis based solely on central negativity as it takes both the even and odd parity CS states simultaneously into account.

We can see that suitable pre-squeezing operation can increase the distance of the states even in the cases when it is practically zero before the corrections. However, unlike the case of central negativity, where the optimal pre-squeezing did depend on the channel transmission only for its high values, here the optimal pre-squeezing changes more or less linearly with the channel transmittance. This shows that there is no single universal guide to protecting the states as different aspects of the states require different methods of protection.

5 Conclusions and outlooks

The loss and noise of bosonic channels deteriorating the non-Gaussian properties of quantum states is one of the main bottlenecks for scalable quantum computation with optical fields. While the noise can be, potentially, compensated by error correction [9–12, 14, 15], this is costly and should come only after other, more feasible avenues, are explored first. We have presented such general mitigation strategy for superposed coherent states based only on feasible Gaussian operations. This operation can be realized either actively, by directly performing the Gaussian operation [58], or it can be incorporated into the state preparation stage of the protocols [35].

It can be straightforwardly extended to mitigate decoherence of the continuous variable component in quantum systems with hybrid entanglement between discrete qubits and continuous-variable CS states [19, 59–61].

While the method is most valuable for optical fields propagating through bosonic channels, the concept is general and can be straightforwardly employed to preserve the non-Gaussian property of quantum states in other bosonic systems, such as microwave cavities, spin systems, trapped ions, or optomechanics [62–69].

Acknowledgements

The authors acknowledge early discussions with H. Le Jeannic. J.P. acknowledges fruitful discussions with O. Solodovnikova. J.P. acknowledges using the computational cluster at the Department of Optics at Palacký University and using several open-source software libraries [70–74] in the computation and subsequent evaluation of presented results.

Funding

We acknowledge Grant No. 22-08772S of the Czech Science Foundation, the European Union’s HORIZON Research and Innovation Actions under Grant Agreement no. 101080173 (CLUSTEC). This work was also supported by the French National Research Agency via the ShoQC Quanterra project (ANR 19-QUAN-0005-05), and via the France 2030 projects QCommTestbed (ANR-22-PETQ-0011) and OQuLus (ANR-22-PETQ-0013). J.L. is a member of the Institut Universitaire de France. In addition, J.P. acknowledges project IGA-PrF-2024-008 of Palacký University.

References

- [1] F. Arute et al. “Quantum supremacy using a programmable superconducting processor”. In: *Nature* 574.7779 (Oct. 2019), pp. 505–510. doi: [10.1038/s41586-019-1666-5](https://doi.org/10.1038/s41586-019-1666-5).
- [2] H. Wang et al. “Boson Sampling with 20 Input Photons and a 60-Mode Interferometer in a 10^{14} -Dimensional Hilbert Space”. In: *Physical Review Letters* 123.25 (Dec. 2019). doi: [10.1103/physrevlett.123.250503](https://doi.org/10.1103/physrevlett.123.250503).
- [3] H.-S. Zhong et al. “Quantum computational advantage using photons”. In: *Science* 370.6523 (Dec. 2020), pp. 1460–1463. doi: [10.1126/science.abe8770](https://doi.org/10.1126/science.abe8770).
- [4] T. Rudolph. “Why I am optimistic about the silicon-photonics route to quantum computing”. In: *APL Photonics* 2.3 (Mar. 2017). doi: [10.1063/1.4976737](https://doi.org/10.1063/1.4976737).
- [5] J. E. Bourassa et al. “Blueprint for a Scalable Photonic Fault-Tolerant Quantum Computer”. In: *Quantum* 5 (Feb. 2021), p. 392. doi: [10.22331/q-2021-02-04-392](https://doi.org/10.22331/q-2021-02-04-392).

- [6] A. Inoue et al. “Toward a multi-core ultra-fast optical quantum processor: 43-GHz bandwidth real-time amplitude measurement of 5-dB squeezed light using modularized optical parametric amplifier with 5G technology”. In: *Applied Physics Letters* 122.10 (Mar. 2023). doi: [10.1063/5.0137641](https://doi.org/10.1063/5.0137641).
- [7] W. Asavanant et al. “Generation of time-domain-multiplexed two-dimensional cluster state”. In: *Science* 366.6463 (Oct. 2019), pp. 373–376. doi: [10.1126/science.aay2645](https://doi.org/10.1126/science.aay2645).
- [8] M. V. Larsen et al. “Deterministic generation of a two-dimensional cluster state”. In: *Science* 366.6463 (Oct. 2019), pp. 369–372. doi: [10.1126/science.aay4354](https://doi.org/10.1126/science.aay4354).
- [9] D. Gottesman et al. “Encoding a qubit in an oscillator”. In: *Physical Review A* 64.1 (June 2001). doi: [10.1103/physreva.64.012310](https://doi.org/10.1103/physreva.64.012310).
- [10] N. C. Menicucci. “Fault-Tolerant Measurement-Based Quantum Computing with Continuous-Variable Cluster States”. In: *Physical Review Letters* 112.12 (Mar. 2014). doi: [10.1103/physrevlett.112.120504](https://doi.org/10.1103/physrevlett.112.120504).
- [11] B. Q. Baragiola et al. “All-Gaussian Universality and Fault Tolerance with the Gottesman-Kitaev-Preskill Code”. In: *Physical Review Letters* 123.20 (Nov. 2019). doi: [10.1103/physrevlett.123.200502](https://doi.org/10.1103/physrevlett.123.200502).
- [12] G. Pantaleoni et al. “Modular Bosonic Subsystem Codes”. In: *Physical Review Letters* 125.4 (July 2020). doi: [10.1103/physrevlett.125.040501](https://doi.org/10.1103/physrevlett.125.040501).
- [13] T. C. Ralph et al. “Quantum computation with optical coherent states”. In: *Physical Review A* 68.4 (Oct. 2003). doi: [10.1103/physreva.68.042319](https://doi.org/10.1103/physreva.68.042319).
- [14] A. P. Lund et al. “Fault-Tolerant Linear Optical Quantum Computing with Small-Amplitude Coherent States”. In: *Physical Review Letters* 100.3 (Jan. 2008). doi: [10.1103/physrevlett.100.030503](https://doi.org/10.1103/physrevlett.100.030503).
- [15] J. Hastrup et al. “All-optical cat-code quantum error correction”. In: *Physical Review Research* 4.4 (Oct. 2022). doi: [10.1103/physrevresearch.4.043065](https://doi.org/10.1103/physrevresearch.4.043065).
- [16] S. Omkar et al. “Resource-Efficient Topological Fault-Tolerant Quantum Computation with Hybrid Entanglement of Light”. In: *Physical Review Letters* 125.6 (Aug. 2020). doi: [10.1103/physrevlett.125.060501](https://doi.org/10.1103/physrevlett.125.060501).
- [17] N. J. Cerf et al. *Quantum Information with Continuous Variables of Atoms and Light*. 2007. doi: [10.1142/p489](https://doi.org/10.1142/p489).
- [18] P. Minzioni et al. “Roadmap on all-optical processing”. In: *Journal of Optics* 21.6 (May 2019), p. 063001. doi: [10.1088/2040-8986/ab0e66](https://doi.org/10.1088/2040-8986/ab0e66).
- [19] G. Guccione et al. “Connecting heterogeneous quantum networks by hybrid entanglement swapping”. In: *Science Advances* 6.22 (May 2020). doi: [10.1126/sciadv.aba4508](https://doi.org/10.1126/sciadv.aba4508).
- [20] T. Darras et al. “A quantum-bit encoding converter”. In: *Nature Photonics* 17.2 (Dec. 2022), pp. 165–170. doi: [10.1038/s41566-022-01117-5](https://doi.org/10.1038/s41566-022-01117-5).
- [21] A. Shinjo et al. “Three-Dimensional Matter-Wave Interferometry of a Trapped Single Ion”. In: *Physical Review Letters* 126.15 (Apr. 2021). doi: [10.1103/physrevlett.126.153604](https://doi.org/10.1103/physrevlett.126.153604).
- [22] A. R. Milne et al. “Quantum Oscillator Noise Spectroscopy via Displaced Cat States”. In: *Physical Review Letters* 126.25 (June 2021). doi: [10.1103/physrevlett.126.250506](https://doi.org/10.1103/physrevlett.126.250506).
- [23] M. Yukawa et al. “Generating superposition of up-to three photons for continuous variable quantum information processing”. In: *Optics Express* 21.5 (Feb. 2013), p. 5529. doi: [10.1364/oe.21.005529](https://doi.org/10.1364/oe.21.005529).

- [24] M. Eaton et al. “Measurement-based generation and preservation of cat and grid states within a continuous-variable cluster state”. In: *Quantum* 6 (July 2022), p. 769. doi: [10.22331/q-2022-07-20-769](https://doi.org/10.22331/q-2022-07-20-769).
- [25] I. Straka et al. “Quantum non-Gaussian Depth of Single-Photon States”. In: *Physical Review Letters* 113.22 (Nov. 2014). doi: [10.1103/physrevlett.113.223603](https://doi.org/10.1103/physrevlett.113.223603).
- [26] A. Mari et al. “Positive Wigner Functions Render Classical Simulation of Quantum Computation Efficient”. In: *Physical Review Letters* 109.23 (Dec. 2012). doi: [10.1103/physrevlett.109.230503](https://doi.org/10.1103/physrevlett.109.230503).
- [27] M. Mićuda et al. “Noiseless Loss Suppression in Quantum Optical Communication”. In: *Physical Review Letters* 109.18 (Nov. 2012). doi: [10.1103/physrevlett.109.180503](https://doi.org/10.1103/physrevlett.109.180503).
- [28] C. N. Gagatsos et al. “Heralded noiseless amplification and attenuation of non-Gaussian states of light”. In: *Physical Review A* 89.6 (June 2014). doi: [10.1103/physreva.89.062311](https://doi.org/10.1103/physreva.89.062311).
- [29] H. M. Chrzanowski et al. “Measurement-based noiseless linear amplification for quantum communication”. In: *Nature Photonics* 8.4 (Mar. 2014), pp. 333–338. doi: [10.1038/nphoton.2014.49](https://doi.org/10.1038/nphoton.2014.49).
- [30] R. Stárek et al. “Experimental quantum decoherence control by dark states of the environment”. In: *New Journal of Physics* 22.9 (Sept. 2020), p. 093058. doi: [10.1088/1367-2630/abb47d](https://doi.org/10.1088/1367-2630/abb47d).
- [31] R. Filip. “Amplification of Schrödinger-cat state in a degenerate optical parametric amplifier”. In: *Journal of Optics B: Quantum and Semiclassical Optics* 3.1 (Jan. 2001), S1–S6. doi: [10.1088/1464-4266/3/1/351](https://doi.org/10.1088/1464-4266/3/1/351).
- [32] A. Serafini et al. “Minimum decoherence cat-like states in Gaussian noisy channels”. In: *Journal of Optics B: Quantum and Semiclassical Optics* 6.6 (May 2004), S591–S596. doi: [10.1088/1464-4266/6/6/019](https://doi.org/10.1088/1464-4266/6/6/019).
- [33] R. Y. Teh et al. “Overcoming decoherence of Schrödinger cat states formed in a cavity using squeezed-state inputs”. In: *Physical Review Research* 2.4 (Dec. 2020). doi: [10.1103/physrevresearch.2.043387](https://doi.org/10.1103/physrevresearch.2.043387).
- [34] R. Filip. “Gaussian quantum adaptation of non-Gaussian states for a lossy channel”. In: *Physical Review A* 87.4 (Apr. 2013). doi: [10.1103/physreva.87.042308](https://doi.org/10.1103/physreva.87.042308).
- [35] H. Le Jeannic et al. “Slowing Quantum Decoherence by Squeezing in Phase Space”. In: *Physical Review Letters* 120.7 (Feb. 2018). doi: [10.1103/physrevlett.120.073603](https://doi.org/10.1103/physrevlett.120.073603).
- [36] R. A. Brewster et al. “Reduced decoherence using squeezing, amplification, and antisqueezing”. In: *Physical Review A* 98.3 (Sept. 2018). doi: [10.1103/physreva.98.033818](https://doi.org/10.1103/physreva.98.033818).
- [37] X. Pan et al. “Protecting the Quantum Interference of Cat States by Phase-Space Compression”. In: *Physical Review X* 13.2 (Apr. 2023). doi: [10.1103/physrevx.13.021004](https://doi.org/10.1103/physrevx.13.021004).
- [38] H. Jeong et al. “Efficient quantum computation using coherent states”. In: *Physical Review A* 65.4 (Mar. 2002). doi: [10.1103/physreva.65.042305](https://doi.org/10.1103/physreva.65.042305).
- [39] D. S. Schlegel et al. “Quantum error correction using squeezed Schrödinger cat states”. In: *Physical Review A* 106.2 (Aug. 2022). doi: [10.1103/physreva.106.022431](https://doi.org/10.1103/physreva.106.022431).
- [40] D. J. Weigand et al. “Generating grid states from Schrödinger-cat states without postselection”. In: *Physical Review A* 97.2 (Feb. 2018). doi: [10.1103/physreva.97.022341](https://doi.org/10.1103/physreva.97.022341).
- [41] H. M. Vasconcelos et al. “All-optical generation of states for “Encoding a qubit in an oscillator””. In: *Optics Letters* 35.19 (Sept. 2010), p. 3261. doi: [10.1364/ol.35.003261](https://doi.org/10.1364/ol.35.003261).
- [42] R. Filip et al. “Detecting Quantum States with a Positive Wigner Function beyond Mixtures of Gaussian States”. In: *Physical Review Letters* 106.20 (May 2011). doi: [10.1103/physrevlett.106.200401](https://doi.org/10.1103/physrevlett.106.200401).

- [43] M. Walschaers. “Non-Gaussian Quantum States and Where to Find Them”. In: *PRX Quantum* 2.3 (Sept. 2021). doi: [10.1103/prxquantum.2.030204](https://doi.org/10.1103/prxquantum.2.030204).
- [44] D. Leibfried et al. “Experimental Determination of the Motional Quantum State of a Trapped Atom”. In: *Physical Review Letters* 77.21 (Nov. 1996), pp. 4281–4285. doi: [10.1103/physrevlett.77.4281](https://doi.org/10.1103/physrevlett.77.4281).
- [45] P. Bertet et al. “Direct Measurement of the Wigner Function of a One-Photon Fock State in a Cavity”. In: *Physical Review Letters* 89.20 (Oct. 2002). doi: [10.1103/physrevlett.89.200402](https://doi.org/10.1103/physrevlett.89.200402).
- [46] K. Laiho et al. “Probing the Negative Wigner Function of a Pulsed Single Photon Point by Point”. In: *Physical Review Letters* 105.25 (Dec. 2010). doi: [10.1103/physrevlett.105.253603](https://doi.org/10.1103/physrevlett.105.253603).
- [47] G. Kirchmair et al. “Observation of quantum state collapse and revival due to the single-photon Kerr effect”. In: *Nature* 495.7440 (2013), pp. 205–209. doi: [10.1038/nature11902](https://doi.org/10.1038/nature11902).
- [48] K. Banaszek et al. “Direct measurement of the Wigner function by photon counting”. In: *Physical Review A* 60.1 (July 1999), pp. 674–677. doi: [10.1103/physreva.60.674](https://doi.org/10.1103/physreva.60.674).
- [49] J. Provazník et al. “Benchmarking photon number resolving detectors”. In: *Optics Express* 28.10 (May 2020), p. 14839. doi: [10.1364/oe.389619](https://doi.org/10.1364/oe.389619).
- [50] F. Nicacio et al. “Phase space structure of generalized Gaussian cat states”. In: *Physics Letters A* 374.43 (2010), pp. 4385–4392. doi: [10.1016/j.physleta.2010.08.076](https://doi.org/10.1016/j.physleta.2010.08.076).
- [51] R. I. Booth et al. “Contextuality and Wigner Negativity Are Equivalent for Continuous-Variable Quantum Measurements”. In: *Physical Review Letters* 129.23 (Nov. 2022). doi: [10.1103/physrevlett.129.230401](https://doi.org/10.1103/physrevlett.129.230401).
- [52] U. Chabaud et al. “Resources for Bosonic Quantum Computational Advantage”. In: *Physical Review Letters* 130.9 (Mar. 2023). doi: [10.1103/physrevlett.130.090602](https://doi.org/10.1103/physrevlett.130.090602).
- [53] H. Buhrman et al. “Quantum Fingerprinting”. In: *Physical Review Letters* 87.16 (Sept. 2001). doi: [10.1103/physrevlett.87.167902](https://doi.org/10.1103/physrevlett.87.167902).
- [54] R. Filip. “Overlap and entanglement-witness measurements”. In: *Physical Review A* 65.6 (June 2002). doi: [10.1103/physreva.65.062320](https://doi.org/10.1103/physreva.65.062320).
- [55] A. K. Ekert et al. “Direct Estimations of Linear and Nonlinear Functionals of a Quantum State”. In: *Physical Review Letters* 88.21 (May 2002). doi: [10.1103/physrevlett.88.217901](https://doi.org/10.1103/physrevlett.88.217901).
- [56] K. L. Pagnell. “Measuring Nonlinear Functionals of Quantum Harmonic Oscillator States”. In: *Physical Review Letters* 96.6 (Feb. 2006). doi: [10.1103/physrevlett.96.060501](https://doi.org/10.1103/physrevlett.96.060501).
- [57] M. Ozawa. “Entanglement measures and the Hilbert–Schmidt distance”. In: *Physics Letters A* 268.3 (2000), pp. 158–160. doi: [10.1016/s0375-9601\(00\)00171-7](https://doi.org/10.1016/s0375-9601(00)00171-7).
- [58] K. Miyata et al. “Experimental realization of a dynamic squeezing gate”. In: *Physical Review A* 90.6 (Dec. 2014). doi: [10.1103/physreva.90.060302](https://doi.org/10.1103/physreva.90.060302).
- [59] A. Cavaillès et al. “Demonstration of Einstein-Podolsky-Rosen Steering Using Hybrid Continuous- and Discrete-Variable Entanglement of Light”. In: *Physical Review Letters* 121.17 (Oct. 2018). doi: [10.1103/physrevlett.121.170403](https://doi.org/10.1103/physrevlett.121.170403).
- [60] K. Huang et al. “Engineering optical hybrid entanglement between discrete- and continuous-variable states”. In: *New Journal of Physics* 21.8 (Aug. 2019), p. 083033. doi: [10.1088/1367-2630/ab34e7](https://doi.org/10.1088/1367-2630/ab34e7).
- [61] H. Le Jeannic et al. “Remote preparation of continuous-variable qubits using loss-tolerant hybrid entanglement of light”. In: *Optica* 5.8 (Aug. 2018), p. 1012. doi: [10.1364/optica.5.001012](https://doi.org/10.1364/optica.5.001012).

- [62] B. Vlastakis et al. “Deterministically Encoding Quantum Information Using 100-Photon Schrödinger Cat States”. In: *Science* 342.6158 (2013), pp. 607–610. doi: [10.1126/science.1243289](https://doi.org/10.1126/science.1243289).
- [63] A. Omran et al. “Generation and manipulation of Schrödinger cat states in Rydberg atom arrays”. In: *Science* 365.6453 (Aug. 2019), pp. 570–574. doi: [10.1126/science.aax9743](https://doi.org/10.1126/science.aax9743).
- [64] Y.-H. Chen et al. “Shortcuts to Adiabaticity for the Quantum Rabi Model: Efficient Generation of Giant Entangled Cat States via Parametric Amplification”. In: *Physical Review Letters* 126.2 (Jan. 2021). doi: [10.1103/physrevlett.126.023602](https://doi.org/10.1103/physrevlett.126.023602).
- [65] I. Shomroni et al. “Optomechanical generation of a mechanical catlike state by phonon subtraction”. In: *Physical Review A* 101.3 (Mar. 2020). doi: [10.1103/physreva.101.033812](https://doi.org/10.1103/physreva.101.033812).
- [66] H. Tan et al. “Generation of macroscopic quantum superpositions of optomechanical oscillators by dissipation”. In: *Physical Review A* 88.2 (Aug. 2013). doi: [10.1103/physreva.88.023817](https://doi.org/10.1103/physreva.88.023817).
- [67] F.-X. Sun et al. “Remote Generation of Magnon Schrödinger Cat State via Magnon-Photon Entanglement”. In: *Physical Review Letters* 127.8 (Aug. 2021). doi: [10.1103/physrevlett.127.087203](https://doi.org/10.1103/physrevlett.127.087203).
- [68] C. Flühmann et al. “Encoding a qubit in a trapped-ion mechanical oscillator”. In: *Nature* 566.7745 (2019), pp. 513–517. doi: [10.1038/s41586-019-0960-6](https://doi.org/10.1038/s41586-019-0960-6).
- [69] Y. Miwa et al. “Exploring a New Regime for Processing Optical Qubits: Squeezing and Unsqueezing Single Photons”. In: *Physical Review Letters* 113.1 (July 2014). doi: [10.1103/physrevlett.113.013601](https://doi.org/10.1103/physrevlett.113.013601).
- [70] C. R. Harris et al. “Array programming with NumPy”. In: *Nature* 585.7825 (Sept. 2020), pp. 357–362. doi: [10.1038/s41586-020-2649-2](https://doi.org/10.1038/s41586-020-2649-2).
- [71] P. Virtanen et al. “SciPy 1.0: fundamental algorithms for scientific computing in Python”. In: *Nature Methods* 17.3 (Feb. 2020), pp. 261–272. doi: [10.1038/s41592-019-0686-2](https://doi.org/10.1038/s41592-019-0686-2).
- [72] L. Dalcin et al. “mpi4py: Status Update After 12 Years of Development”. In: *Computing in Science & Engineering* 23.4 (July 2021), pp. 47–54. doi: [10.1109/mcse.2021.3083216](https://doi.org/10.1109/mcse.2021.3083216).
- [73] J. D. Hunter. “Matplotlib: A 2D Graphics Environment”. In: *Computing in Science & Engineering* 9.3 (2007), pp. 90–95. doi: [10.1109/mcse.2007.55](https://doi.org/10.1109/mcse.2007.55).
- [74] A. Meurer et al. “SymPy: symbolic computing in Python”. In: *PeerJ Computer Science* 3 (Jan. 2017), e103. doi: [10.7717/peerj-cs.103](https://doi.org/10.7717/peerj-cs.103).

Supplementary material

Adapting coherent-state superpositions in noisy channels

Jan Provazník^{1*}, Petr Marek¹, Julien Laurat², Radim Filip¹

¹ Department of Optics, Palacký University, 17. listopadu 1192/12, 771 46 Olomouc, Czech Republic

² Laboratoire Kastler Brossel, Sorbonne Université, CNRS, ENS-Université PSL, Collège de France, 4 place Jussieu, 75005 Paris, France

* provaznik@optics.upol.cz

S.1 Conditions for presence of negativity in Wigner functions

It is convenient to rewrite the complex-exponential form of the output Wigner function of the CS state into its manifestly real form. The coefficients $f_X, f_P, \sigma_X, \sigma_P, V_X$ and V_P are all real and positive.

$$W'_{\xi, \pm}(X', P') = 2f_{\pm} \exp\left(-\frac{X'^2}{V_X} - \frac{P'^2}{V_P}\right) \left\{ \exp\left(-\frac{f_X^2}{V_X} X_0^2 - \frac{f_P^2}{V_P} P_0^2\right) \cosh\left(2\left[\frac{f_X}{V_X} X_0 X' + \frac{f_P}{V_P} P_0 P'\right]\right) \pm \exp\left(-\frac{\sigma_X}{V_X} P_0^2 - \frac{\sigma_P}{V_P} X_0^2\right) \cos\left(2\left[\frac{f_P}{V_P} X_0 P' - \frac{f_X}{V_X} P_0 X'\right]\right) \right\}, \quad (\text{S.1})$$

where the factors f_{\pm} stand for the normalization, given as

$$f_{\pm}^{-1} = 2\pi\sqrt{V_X V_P} \left(1 \pm \exp(-X_0^2 - P_0^2)\right). \quad (\text{S.2})$$

Let us begin with the **sufficient and necessary** condition for the existence of any negative area in the Wigner function of the odd-parity CS state. It is only natural to consider the central negativity in this particular case. The formula (S.1) simplifies into

$$W'_{\xi, -}(0, 0) = 2f_- \left\{ \exp\left(-\frac{f_X^2}{V_X} X_0^2 - \frac{f_P^2}{V_P} P_0^2\right) - \exp\left(-\frac{\sigma_X}{V_X} P_0^2 - \frac{\sigma_P}{V_P} X_0^2\right) \right\} \quad (\text{S.3})$$

This expression will be negative if and only if

$$\exp\left(-\frac{f_X^2}{V_X} X_0^2 - \frac{f_P^2}{V_P} P_0^2\right) - \exp\left(-\frac{\sigma_X}{V_X} P_0^2 - \frac{\sigma_P}{V_P} X_0^2\right) < 0, \quad (\text{S.4})$$

that is, if and only if, the second exponential is greater than the first one. Comparing their arguments directly reveals the condition

$$-X_0^2 \left(\frac{f_X f_P - \sigma_X \sigma_P}{V_X V_P}\right) - P_0^2 \left(\frac{f_X f_P - \sigma_X \sigma_P}{V_X V_P}\right) < 0 \iff f_X f_P - \sigma_X \sigma_P > 0. \quad (\text{S.5})$$

The central point of the odd-parity CS state will be negative if and only if $f_X f_P - \sigma_X \sigma_P > 0$. Notably this inequality does not depend on the state. It depends solely on the channel. This concludes the proof for the odd-parity state. ■

The condition for even-parity states is slightly harder to obtain. Once again, we note that we are only interested in a **necessary** condition for existence of negativity anywhere within the Wigner function. In other words, we are looking for a condition that, if violated, will preclude existence of any negativity within the Wigner function. This allows us to be somewhat liberal in the manipulation of the expression (S.1).

We begin with the observation that there are infinitely many (X', P') pairs that satisfy

$$\pm \cos \left(2 \left[\frac{f_P}{V_P} X_0 P' - \frac{f_X}{V_X} P_0 X' \right] \right) \equiv - \left| \cos \left(2 \left[\frac{f_P}{V_P} X_0 P' - \frac{f_X}{V_X} P_0 X' \right] \right) \right|. \quad (\text{S.6})$$

The rest of the proof assumes the Wigner function (S.1) is evaluated only at points of the phase space that satisfy this condition. With this assumption in mind, we can rewrite the curly braced expression from (S.1) into

$$\exp(A) \cosh(B) - \exp(C) |\cos(D)| < 0 \quad (\text{S.7})$$

where we have substituted the arguments of the exponential, geometric and hyperbolic functions for simplicity. Since the hyperbolic cosine is always positive and lower bound by 1, we have

$$\begin{aligned} \exp(A) \cosh(B) - \exp(C) |\cos(D)| < 0 &\iff \\ \exp(A) < \exp(C) \frac{|\cos(D)|}{\cosh(B)} &\iff \\ \exp(A) < \exp(C) &\iff \\ -X_0^2 \left(\frac{f_X f_P - \sigma_X \sigma_P}{V_X V_P} \right) - P_0^2 \left(\frac{f_X f_P - \sigma_X \sigma_P}{V_X V_P} \right) < 0 &\iff \\ \boxed{f_X f_P - \sigma_X \sigma_P > 0}. \end{aligned} \quad (\text{S.8})$$

Where we obtained the third inequality $\exp(A) < \exp(C)$ as an upper bound on the right hand side of the second one. The condition $f_X f_P - \sigma_X \sigma_P > 0$ then follows. This condition, while valid for both even and odd parity CS states, is merely a **necessary** condition for the existence of some negative point. In other words, if violated, there will be **no** negative area at all. ■

S.2 Closed form formula for the Hilbert-Schmidt distance

We derive the closed form formula for the Hilbert-Schmidt distance [57] between the opposite-parity CS states used in the paper. In particular, we have

$$\begin{aligned} \Delta_\xi &= 2\pi \iint_{\mathbb{R}^2} \left[W'_{\xi,+}(X', P') - W'_{\xi,-}(X', P') \right]^2 dX' dP' \\ &= P_{\xi,+} - 2Q_\xi + P_{\xi,-} \end{aligned} \quad (\text{S.9})$$

where the expressions for purity and the mutual overlap read

$$\begin{aligned}
P_{\xi, \pm} &= 2\pi \iint_{\mathbb{R}^2} W_{\xi, \pm}^2(X, P) dX dP \\
&= \frac{1}{\sqrt{V_X V_P}} \frac{1 + M + N \pm 4L}{2 \left(1 \pm \exp[-X_0^2 - P_0^2]\right)^2} \\
O_{\xi} &= 2\pi \iint_{\mathbb{R}^2} W_{\xi, +}(X, P) W_{\xi, -}(X, P) dX dP \\
&= \frac{1}{\sqrt{V_X V_P}} \frac{1 + M - N}{2 \left(1 - \mu \exp[-2X_0^2 - 2P_0^2]\right)}.
\end{aligned} \tag{S.10}$$

The individual factors in both expressions were obtained directly by computing the underlying Gaussian integrals. Their closed forms are

$$\begin{aligned}
M &= \exp\left(-2\frac{f_X^2}{V_X}X_0^2 - 2\frac{f_P^2}{V_P}P_0^2\right) \\
N &= \exp\left(-2X_0^2 - 2P_0^2\right) + \exp\left(-2\frac{\sigma_X}{V_X}P_0^2 - 2\frac{\sigma_P}{V_P}X_0^2\right) \\
L &= \exp\left(-\left[\frac{f_X^2}{2V_X} + \frac{f_P^2}{2V_P} + \frac{\sigma_P}{V_P}\right]X_0^2 - \left[\frac{f_X^2}{2V_X} + \frac{f_P^2}{2V_P} + \frac{\sigma_X}{V_X}\right]P_0^2\right) \times \\
&\quad \cos\left(X_0\left[\frac{f_X^2}{V_X} + \frac{f_P^2}{V_P}\right]P_0\right)
\end{aligned} \tag{S.11}$$

where we use $V_{\bullet} = \sigma_{\bullet} + f_{\bullet}^2$ with $(\bullet \in \{X, P\})$ for clarity and improved readability.